The Astrophysical Journal, 661: L199–L202, 2007 June 1

PHOTOLYTICALLY GENERATED AEROSOLS IN THE MESOSPHERE AND THERMOSPHERE OF TITAN

Mao-Chang Liang,[1,2] Yuk L. Yung,[2] and Donald E. Shemansky[3]
Received 2006 November 20; accepted 2007 April 11; published 2007 May 8

ABSTRACT

Analysis of the *Cassini* Ultraviolet Imaging Spectrograph (UVIS) stellar and solar occultations at Titan to date include 12 species: N_2 (nitrogen), CH_4 (methane), C_2H_2 (acetylene), C_2H_4 (ethylene), C_2H_6 (ethane), C_4H_2 (diacetylene), C_6H_6 (benzene), C_6N_2 (dicyanodiacetylene), C_2N_2 (cyanogen), HCN (hydrogen cyanide), HC_3N (cyanoacetylene), and aerosols distinguished by a structureless continuum extinction (absorption plus scattering) of photons in the EUV. The introduction of aerosol particles, retaining the same refractive index properties as tholin with radius ~125 Å and using Mie theory, provides a satisfactory fit to the spectra. The derived vertical profile of aerosol density shows distinct structure, implying a reactive generation process reaching altitudes more than 1000 km above the surface. A photochemical model presented here provides a reference basis for examining the chemical and physical processes leading to the distinctive atmospheric opacity at Titan. We find that dicyanodiacetylene is condensable at ~650 km, where the atmospheric temperature minimum is located. This species is the simplest molecule identified to be condensable. Observations are needed to confirm the existence and production rates of dicyanodiacetylene.

Subject headings: atmospheric effects — methods: data analysis — methods: numerical — planetary systems — planets and satellites: individual (Titan) — radiative transfer

1. INTRODUCTION

Titan is nature's laboratory for organic synthesis. The major molecules in the atmosphere are N_2 and CH_4. The coupled chemistry between nitrogen and carbon leads to high abundances of nitrogen/carbon compounds, such as hydrogen cyanide (see, e.g., Yung et al. 1984; Coustenis et al. 2003; Wilson & Atreya 2004). This is caused primarily by the low gravity of Titan that allows hydrogen to escape readily (e.g., Yelle et al. 2006), resulting in low hydrogen abundance and rich hydrocarbon production. When the order of hydrocarbons and nitriles is large enough, they condense to form aerosols and precipitate. The stratosphere is a major region for the production of haze (e.g., McKay et al. 2001). The estimated vertically integrated rate is $(0.5–2) \times 10^{-14}$ g cm^{-2} s^{-1}, with haze formation taking place in the 300–500 km region. Total mass loading according to McKay et al. (2001) was about 250 mg m^{-2}, made by molecules with a C/N ratio of 2–4 and a C/H ratio of about unity. The present work obtains about 100 mg m^{-2} (assuming density 3 g cm^{-3}) above 300 km.

2. *CASSINI* UVIS OBSERVATIONS

On 2004 December 13, the *Cassini* UVIS recorded the occultation of two stars, λ Sco (Shaula; latitude −36°) and α Vir (Spica; latitude range of +63° and +48°), near the end of the second Titan flyby (T_B) (details are referred to Shemansky et al. 2005; Shemansky 2006; and D. E. Shemansky et al. 2007, in preparation). The fully reduced results from λ Sco only are referenced here. The vertical distribution of the aerosol component as the terminal product of N_2/CH_4 physical and chemical processes is of primary interest to this Letter. The spectral region 1850–1900 Å (SP1) is effectively free of the measurable hydrocarbon and cyano species in this atmosphere apart from aerosols, and this region is used photometrically to trace the aerosol structure. The vertical profile of extinction for SP1 below 1000 km was carried out at the highest possible ray-height resolution (3–5 km) in order to reveal possible structure in the distribution.

The best fit to the transmission spectrum at impact parameter $h = 514$ km is shown in Figure 1 as an example of spectral reduction. Table 1 shows the extracted line-of-sight abundances from this element of the occultation. Figure 2 shows the aerosol density vertical distribution (*filled circles*) derived from the reduction of the λ Sco occultation, compared to the derived CH_4 profile (*dashed line*). The reduced data extend from $h = 330$ to 970 km, where the signal noise terminates the reduction (see D. E. Shemansky et al. 2007, in preparation, for details). The remarkable property of the aerosol distribution is the sudden departure from tracking the CH_4 abundance at $h = 468$ km toward higher altitudes. The interval between 468 and 550 km, where abundance remains approximately constant, is interpreted as a primary aerosol source region. The density extraction is a direct deconvolution of the abundance distribution. The derivation is based on assumed spherical uniformity and assumed uniformity in composition with altitude. The observations show measurable simple scattering in the 1800 Å region at $h = 1250$ km, indicating that aerosols are extensively distributed into the thermosphere.

The cross sections for extinction of UV light by aerosols were computed using the complex refractive index measured by Khare et al. (1984) for solid-state tholins and the scattering code of Mishchenko & Travis (1998). Representative complex indices of refraction at 588, 1215, 1631, and 2384 Å are (0.963, 0.62), (1.74, 0.37), (1.65, 0.24), and (1.68, 0.21), respectively. Assuming a mean radius of 125 Å for aerosols, the corresponding extinction cross sections are 2.4×10^{-12}, 3.9×10^{-13}, 2.0×10^{-13}, and 1.2×10^{-13} cm^2, respectively. The actual computation used in this work has a finer wavelength grid. Note that the current UVIS data set no constraint on the vertical variation of the optical property of aerosols.

Extinction of the EUV stellar photons is dominated by CH_4 in the 1100–1400 Å region. At longer wavelengths, the structure is a combination of the higher order hydrocarbon and cyano

[1] Research Center for Environmental Changes, Academia Sinica, Taipei 115, Taiwan.
[2] Division of Geological and Planetary Sciences, California Institute of Technology, Pasadena, CA 91125.
[3] Planetary and Space Science Division, Space Environment Technologies, Pasadena, CA 91107.

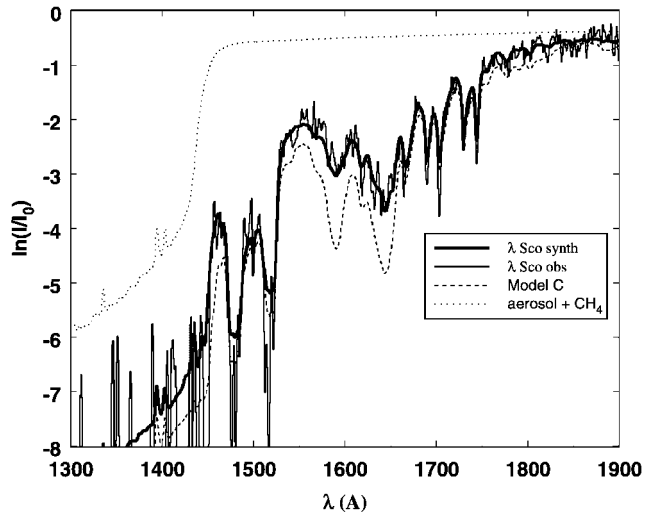

FIG. 1.—The transmission spectrum of the UVIS λ Sco occultation integrated over the impact parameter 514–537 km (*thin solid line*), compared to the best-fit synthesis (D. E. Shemansky et al. 2007, in preparation) using the combined identified species (*thick solid line*) and to model C from the present physical chemistry code (*dashed line*). The dotted line shows the aerosol component combined with the CH_4 absorber in this reduction. The CH_4 absorber ($\lambda <$ 1490 Å) is included with aerosol here as a means of including a large part of the impact of the instrument point-spread function on the fitting process. The optical depth in region SP1 is entirely attributed to aerosol extinction; the small difference between the observed data and the aerosol component at SP1 is an artifact of the UVIS EUV instrument point-spread function. The abundances of the species for this case are given in Table 1 (see text).

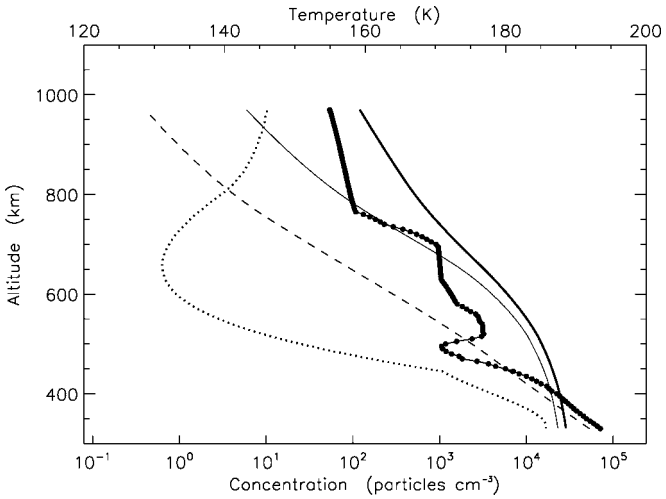

FIG. 2.—Aerosol density (*filled circles*) derived from the UVIS λ Sco occultation compared to the CH_4 (*dashed line*) scaled by 10^{-9} (Shemansky et al. 2005; Shemansky 2006). The increase of the mixing ratio of the UVIS aerosols through the mesosphere to at least 1000 km implies that the production of aerosols must take place at significant rates throughout the mesosphere and thermosphere. The UVIS-derived temperature profile is shown by the dotted line, which reflects a correction to the one presented by Shemansky et al. (2005). The model aerosol profiles are shown by the thin and thick solid lines (see text). The over- and underestimations are due to the fact that we assume a constant sedimentation velocity of 0.25 cm s^{-1}, calculated at 535 km (Cabane et al. 1992).

species. The C_6H_6 cross section peaks at 1759.9–1815.1 Å, blended primarily with C_2H_4. Dicyanodiacetylene has a cross section peak in the SP1 spectral region. Dicyanodiacetylene and benzene have not been detected in the absorption spectra (D. E. Shemansky et al. 2007, in preparation). Aerosol extinction is detectable at ~970 km in the transmission spectra and dominates all absorbers at all wavelengths in the UVIS except for CH_4, at altitudes below 400–450 km.

Figure 1 shows the contribution of aerosol extinction to the total measured optical depth at 514 km. In the spectral region SP1 aerosol extinction is entirely responsible for the optical depth. The measurable spectral region for extracting the aerosol component is 1500–1900 Å, where the wavelength dependence of extinction shows a proportionality to $\lambda^{-1.5}$. The *Voyager* and *Cassini* photometric observations in the UV spectral region (Porco et al. 2005; West et al. 2006) have revealed the presence of detached haze layers at Titan. The *Cassini* results show the presence of a latitudinally uniform detached layer near 500 km in forward-scattered 3380 Å photons. The relationship of this phenomenon to the aerosols identified here requires further investigation. A comparison to *Voyager* results (Smith et al. 1982) shows that the major differences are that the apparent strong extinction by aerosols takes effect about 100 km higher for *Voyager* and that significantly more extinction is evident for *Voyager* in the 700–1000 km region. The *Voyager* data show a broad extinction maximum near 770 km.

TABLE 1
SUMMARY OF MODEL RESULTS

Molecule	*Cassini*	Model A	Model B	Model C	Model D	WA04
N_2 ($\times 10^{21}$)	5.8	5.8	5.8	5.8	5.8	5.8
CH_4 ($\times 10^{19}$)	6.0	15	9.4	9.5	9.7	13
C_2H_2 ($\times 10^{17}$)	2.1	15	9.1	1.9	1.7	1.5
C_2H_4 ($\times 10^{16}$)	4.0	9.3	5.7	4.0	2.0	3.4
C_2H_6 ($\times 10^{16}$)	7.0	200	110	17	9.2	20
HCN ($\times 10^{17}$)	1.0	5.6	3.7	0.69	0.53	0.017
C_4H_2 ($\times 10^{15}$)	4.5	59	37	12	2.1	41
C_6N_2 ($\times 10^{14}$)	<1.0	15	16	5.7	8.0	...
C_6H_6 ($\times 10^{14}$)	<1.4	18	13	12	0.041	0.21
HC_3N ($\times 10^{15}$)	<3.9	27	25	6.9	7.8	0.96
C_2N_2 ($\times 10^{15}$)	<4.0	0.84	1.2	0.34	0.42	0.00035
Tholin ($\times 10^{11}$)	4.6	...	...	...	...	...

NOTES.—Values are line-of-sight column-integrated abundances, in units of molecules cm^{-2}, reported by matching the observed N_2 abundance. Model A: Hydrostatic atmosphere. Model B: Nonhydrostatic atmosphere, an ad hoc downward wind, and extinction due to the derived tholins are assumed (see text). Model C: Same as model B, but with additional sinks for the tabulated nine photochemical species (see text). Model D: Same as model C, but with the updated hydrocarbon chemistry from Moses et al. (2005). WA04: Model results from Wilson & Atreya (2004). Note that, in this Letter, the microphysical processes of C_6N_2 are not solved self-consistently, and hence the tabulated abundances of C_6N_2 do not reflect the removal by condensation.

TABLE 2
CHEMICAL REACTIONS TO C_6N_2

Label	Reactants	Products	Reactions[a]	Rate Coefficients[b]	Ref.
R454	$HC_5N + h\nu$	$C_4H + CN$	$J(HC_3N + h\nu \rightarrow C_2H + CN)$	1.8×10^{-8}	1
R455	$HC_5N + h\nu$	$C_5N + H$	$J(HC_3N + h\nu \rightarrow C_3N + H)$	3.3×10^{-8}	1
R456	$C_6N_2 + h\nu$	$C_5N + CN$	$J(C_4N_2 + h\nu \rightarrow C_3N + CN)$	3.0×10^{-7}	2
R492	$C_3N + HC_3N$	$C_6N_2 + H$	$k(C_2H + C_2H_2 \rightarrow C_4H_2 + H)$	$8.6 \times 10^{-16} T^{1.8} e^{474/T}$	3
R495	$CN + C_4H_2$	$HC_5N + H$	$k(CN + C_2H_2 \rightarrow HC_3N + H)$	2.3×10^{-11}	2
R496	$CN + HC_5N$	$C_6N_2 + H$	$k(CN + HC_3N \rightarrow C_4N_2 + H)$	1.0×10^{-11}	2
R497	$C_5N + CH_4$	$HC_5N + CH_3$	$k(C_3N + CH_4 \rightarrow HC_3N + CH_3)$	5.0×10^{-14}	2
R498	$C_5N + C_2H_6$	$HC_5N + C_2H_5$	$k(C_3N + C_2H_6 \rightarrow HC_3N + C_2H_5)$	1.0×10^{-11}	2

REFERENCES.—(1) Lebonnois et al. (2001) and Wilson & Atreya (2004); (2) Yung (1987); (3) Lebonnois et al. (2001) and Opansky & Leone (1996).

[a] Estimated from the quoted reactions. Units are s^{-1} for photolysis reactions (J) and $cm^3\ s^{-1}$ for two-body reactions (k). The photolysis rate coefficients are given at the top of the model atmosphere.

[b] The values are taken from model C. T is the atmospheric temperature.

3. PHOTOCHEMICAL MODELING

Vertical profiles of the major species have been calculated using a photochemical model. The photochemical reactions are taken from Yung et al. (1984), Yung (1987), and Moses et al. (2000). The chemical scheme to C_6N_2 is hypothesized to be similar to that to C_4N_2, as derived by Yung (1987) and summarized in Table 2. The temperature profile is based on the *Cassini* measurements (Fig. 2, *dotted line*). The vertical eddy mixing profile is taken from Yung et al. (1984). The model simulation is diurnally averaged at low latitude. The incident UV flux is the mean between solar maximum and minimum. Table 1 provides a summary of model results. Sensitivity to the selection of hydrocarbon kinetics and that of kinetics and vertical eddy coefficients are shown by models D and WA04, respectively.

We fix the N_2 abundance to that derived from the *Cassini* measurements. The model starts with a hydrostatic atmosphere. With the prescribed vertical diffusion coefficients and taking the photolysis of CH_4 into account, the abundance of CH_4 is overestimated (see Table 1), compared with the measurements. To bring the model into better agreement with the observations, we introduce an ad hoc advection that transports species other than N_2 downward. The wind is prescribed with strength proportional to the inverse of the square root of atmospheric density. The wind speed reaches -20 cm s^{-1} at the top of the model atmosphere (~1500 km). The assumed downward wind is qualitatively consistent with global circulation that has a downward transport at mid to high latitudes (e.g., Lebonnois et al. 2001). A comparison with modeled CH_4 abundances between models A and C is shown in Figure 3. We note that dynamics plays an important role in distributing photochemical products (e.g., Lebonnois et al. 2001), especially in the regions above ~500 km (the regions of interest to this work) where the transport time is, in general, shorter than the chemical removal time of hydrocarbon and cyano species (e.g., Wilson & Atreya 2004); current simulations coupled with dynamics and photochemistry are limited to the regions below ~400 km (Lebonnois et al. 2001). The latitudinal variations of hydrocarbon and cyano abundances (e.g., Flasar et al. 2005) are the consequence of atmospheric transport and photochemical processes.

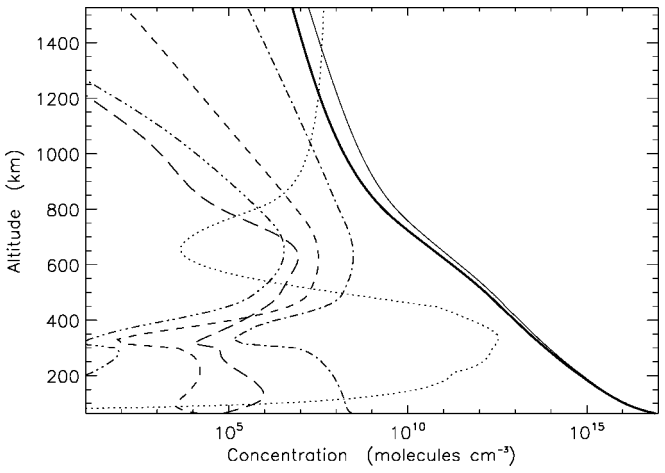

FIG. 3.—Modeled (model C) vertical profiles for CH_4 (*thick solid line*), HC_3N (*dashed line*), HCN (*dash-dotted line*), C_6N_2 (*double–dot-dashed line*), and C_6H_6 (*long-dashed line*). The thin solid line represents modeled CH_4 by model A. The saturation density of C_6N_2 extrapolated from high-temperature measurements (295–369 K; Saggiomo 1957) is shown by the dotted line. The resulting H_2 (3×10^{-3}) and CH_4 (2.3%) mixing ratios at 1174 km and H_2 escape flux (7×10^9 molecules $cm^{-2}\ s^{-1}$) at the top are in good agreement with the observations [$(4 \pm 1) \times 10^{-3}$, 2.7% ± 0.1%, and $(1.2 \pm 0.2) \times 10^{10}$ molecules $cm^{-2}\ s^{-1}$, respectively; Yelle et al. 2006].

The modeled profiles of HCN, HC_3N, C_6H_6, and C_6N_2 are presented in Figure 3. Calculated abundances are compared to extraction from observation at 514 km in Table 1. Comparisons between models and observations at other impact parameters will be deferred to a later paper. The results for five variations on the model at this impact parameter are given in Table 1. In general, our base models (models A and B) overestimate the abundances of hydrocarbons by as much as 10 times. An indication of the difference in the predicted model C and observed optical depth spectra is shown in Figure 1. Model C (Table 1) is too high relative to measured abundance in C_2H_6 and C_4H_2. The modeled C_6N_2, C_6H_6, and HC_3N are also well above the upper limits set by observation. There are two ways of reducing the abundances. (1) One way is through faster transport of photochemical products to the lower atmosphere, as in the model of Wilson & Atreya (2004; model WA04). Comparing the transport time constant with the chemical destruction time, the abundances of C_2H_2, C_2H_6, HCN, and C_2N_2 have a sensitivity to transport, and those of C_2H_4, C_4H_2, C_6N_2, C_6H_6, and HC_3N at ~500 km are close to being in photochemical equilibrium (e.g., Wilson & Atreya 2004). (2) Another way is through relatively rapid two-body physicochemical processes forming aerosols as simulated in models C and D. The loss rates in these models are assumed to be proportional to the physical collision rates between aerosols (with radius 125 Å) and molecules; adsorption reactions are assumed for all photochemical species listed in Table 1. The aerosol density is from Figure 2. The adsorption efficiency for this absolute loss, an assumed value of 0.01, yields the concentrations shown in

Table 1. As described below, this process is required for explaining the aerosol abundance shown in Figure 2.

4. DISCUSSION

The source of aerosols has long been a puzzle in the atmosphere of Titan. It is generally believed that the synthesis of increasingly complex hydrocarbon and nitrogen compounds will eventually lead to saturation, resulting in coagulation and precipitation. However, the chemical composition of the condensable species has not yet been established. In this Letter, we propose that the simplest condensable compound is C_6N_2. The abundances of the higher order species in the UVIS observations are significantly lower than the present model calculations. Assuming that the model conversion rates for the CH_4 source are basically correct, there is an implied loss rate for these species that is substantially higher than the model provides. The model calculation contains an absolute loss to the measured aerosols using a conservatively small adsorption probability. If a significant fraction of the implied loss is delivered to the production of aerosols, the model can be adjusted by assuming a larger irreversible adsorption probability and a consequent higher precipitation rate for the aerosols. This will bring the model abundances into better conformance with observation but will not necessarily resolve differences in partitioning, and may not resolve issues raised in regard to rate limits for the mass flow process that cycles to the surface. We propose that the aerosol formation is initiated by the condensation of C_6N_2 and the adsorption to external meteoritic dust; both serve as seeds for aerosol formation. The subsequent physical processes of adsorption on the existing aerosols and (photo)chemistry converting these clusters into refractory tholins constitute the production and maintenance of the aerosol distribution. Hunten (2006) has recently proposed that haze is a major sink of ethane at Titan. The process of formation of aerosols requires the stable adsorption of the higher order hydrocarbon and nitrile species.

The production rate of C_6N_2 in the model limits the production rate of aerosols from this direct path. The saturation density of dicyanodiacetylene shown in Figure 3 shows that condensation can take place between ~550 and 800 km. The volume production rate of C_6N_2 in this region is quite uniform (~1 molecules cm^{-3} s^{-1}); the column-integrated (550–800 km) rate is ~10^7 molecules cm^{-2} s^{-1}, or ~2×10^{-15} g cm^{-2} s^{-1}. This contribution is a small fraction of the total aerosol production but is extremely important as a source of condensation nuclei. The maximum rate of aerosol production, however, is set by the total photolysis rate of CH_4, which is on the order of 10^{10} molecules cm^{-2} s^{-1}, or 2×10^{-13} g cm^{-2} s^{-1} of carbon, a result that is independently corroborated by the H_2 escape flux (Yelle et al. 2006). The rate of removal of molecules by the existing particles in model C is close to this maximum rate. However, the resulting aerosol profile (thin solid line in Fig. 2) underestimates the observed aerosol abundances above ~800 km, suggesting an additional source at the top of the atmosphere, equivalent to a downward flux of 5×10^{-14} g cm^{-2} s^{-1} (*thick solid line*). This flux is consistent with that inferred from the *Cassini* Ion Neutral Mass Spectrometer measurements (Waite et al. 2007) on the basis of ion chemistry not considered here. Note that a sedimentation velocity of 0.25 cm s^{-1} has to be imposed in order to match the observed aerosol profile; this implies that the radius of the aerosols must be ~125 Å in the mesosphere and thermosphere.

We emphasize that there are significant uncertainties in rate process quantities and that stronger constraints are needed. Laboratory measurements for the adsorption rates on aerosols in collision with the high-order molecules are required to verify this process and to provide a better constraint to the aerosol mass loading in the atmosphere of Titan. In addition, the photochemical paths to high-order hydrocarbon and nitrile compounds such as C_6N_2 and C_6H_6 are speculative. Atmospheric dynamics in the mesosphere of Titan also plays a central role in molecule/aerosol mixing. Further laboratory measurements and *Cassini* observations will provide us with valuable information for refining our understanding of the chemical, dynamical, and microphysical processes in the atmosphere of Titan.

This research was supported by NASA grant NNG06GF33G and *Cassini* grant JPL.1256000 to the California Institute of Technology. D. E. S. acknowledges support from NASA grant NNG06GH76G and from *Cassini* UVIS Program contract 1531660 to Space Environment Technologies.

REFERENCES

Cabane, M., Chassefiere, E., & Israel, G. 1992, Icarus, 96, 176
Coustenis, A., Salama, A., Schulz, B., Ott, S., Lellouch, E., Encrenaz, T., Gautier, D., & Feuchtgruber, H. 2003, Icarus, 161, 383
Flasar, F. M., et al. 2005, Science, 308, 975
Hunten, D. M. 2006, Nature, 443, 669
Khare, B. N., Sagan, C., Arakawa, E. T., Suits, F., Callcott, T. A., & Williams, M. W. 1984, Icarus, 60, 127
Lebonnois, S., Toublanc, D., Hourdin, F., & Rannou, P. 2001, Icarus, 152, 384
McKay, C. P., Coustenis, A., Samuelson, R. E., Lemmon, M. T., Lorenz, R. D., Cabane, M., Rannou, P., & Drossart, P. 2001, Planet. Space Sci., 49, 79
Mishchenko, M. I., & Travis, L. D. 1998, J. Quant. Spectrosc. Radiat. Transfer, 60, 309
Moses, J. I., Bezard, B., Lellouch, E., Gladstone, G. R., Feuchtgruber, H., & Allen, M. 2000, Icarus, 143, 244
Moses, J. I., Fouchet, T., Bezard, B., Gladstone, G. R., Lellouch, E. & Feuchtgruber, H. 2005, J. Geophys. Res., 110, E08001
Opansky, B. J., & Leone, S. R. 1996, J. Phys. Chem., 100, 4888
Porco, C. C., et al. 2005, Nature, 434, 159
Saggiomo, A. J. 1957, J. Organic Chem., 22, 1171
Shemansky, D. E. 2006, in Abstracts of 36th COSPAR Scientific Assembly, 2006 July 16–23, Beijing, China (Paris: COSPAR), 2748
Shemansky, D. E., Stewart, A. I. F., West, R. A., Esposito, L. W., Hallett, J. T., & Liu, X. M. 2005, Science, 308, 978
Smith, G. R., Strobel, D. F., Broadfoot, A. L., Sandel, B. R., Shemansky, D. E., &Holberg, J. B. 1982, J. Geophys. Res., 87, 1351
Waite, J. H., Jr., Young, D. T., Cravens, T. E., Coates, A. J., Crary, F. J., Magee, B., & Westlake, J. 2007, Science, in press
West, R. A., et al. 2006, BAAS, 38, 22.02
Wilson, E. H., & Atreya, S. K. 2004, J. Geophys. Res., 109, E06002
Yelle, R. V., Borggren, N., de la Haye, V., Kasprzak, W. T., Niemann, H. B., Müller-Woodarg, I., & Waite, J. H., Jr. 2006, Icarus, 182, 567
Yung, Y. L. 1987, Icarus, 72, 468
Yung, Y. L., Allen, M., & Pinto, J. P. 1984, ApJS, 55, 465